An Exact Near-Field Model Based Localization for Bistatic MIMO Radar with COLD arrays

Hua Chen, *Member, IEEE*, Weilong Wang, Wei Liu, *Senior Member, IEEE*,
Ye Tian, *Member, IEEE* and Gang Wang, *Senior Member, IEEE*

***Abstract*—Most existing near-field (NF) source localization algorithms are developed based on the Fresnel approximation model, and assume that the spatial amplitudes of the target at the sensors are equal. Unlike these algorithms, an NF source parameter estimation algorithm is proposed, based on the exact spatial propagation geometry model, for bistatic multiple-input multiple-output (MIMO) radar deployed with a linear concentered orthogonal loop and dipole (COLD) array at both the transmitter and receiver. The proposed method first compresses the output signal of the matched filter at the receiver into a third-order parallel factor (PARAFAC) data model, on which a trilinear decomposition is performed, and subsequently three factor matrices can be obtained. Then, multiple parameters of interest, including direction-of-departure (DOD), direction-of-arrival (DOA), range from transmitter to target (RFTT), range from target to receiver (RFTR), two-dimensional (2-D) transmit polarization angle (TPA) and 2-D receive polarization angle (RPA), are estimated from the spatial amplitude ratio exploiting the rotation invariant property and the Khatri-Rao product. Finally, the phase uncertainties of transmit and receive arrays can be extracted from additional phase items. The proposed algorithm avoids spectrum peak search, and the estimated parameters in closed forms can be automatically matched unambiguously. In addition, it is suitable for non-uniform linear arrays (NLA) with arbitrary array element spacing and phase uncertainty. Advantages of the proposed method are demonstrated by simulation results.**

***Index Terms*—MIMO radar, Near-field, COLD array, parallel factor, spatial amplitude ratio.**

I. Introduction

Compared to the traditional phased array radar, multiple-input multiple-output (MIMO) radar can achieve a significantly improved performance by exploiting waveform diversity and spatial diversity [1–3]. There are different designs for MIMO radar depending on layouts of the transmit array and receive array, and in this work, we focus on the bistatic MIMO radar.

Many methods have been proposed for target localization and parameter estimation in bistatic MIMO radar. In [4], a reduced-dimension multiple signal classification (MUSIC) algorithm was proposed to jointly estimate the direction of departure (DOD) and direction of arrival (DOA) of the targets, but it involves spectral peak search operations which are computationally demanding. By making use of the rotation invariant property, estimation of signal parameters via rotational invariance technique (ESPRIT)-based algorithms were presented to jointly estimate the transceiver angles [5, 6], where no spectral peak search is required. In [7], a method for joint estimation of DOD and DOA based on parallel factor (PARAFAC) decomposition was proposed, in which automatically paired DOAs and DOAs are achieved by exploiting the strong algebraic structure of array measurements. However, all the above algorithms assume that the targets are located in the far-field (FF), and the impinging wavefront is planar.

When the target is located in the near-field (NF), the signal wavefront becomes spherical and the range information of the target should be considered. For NF source localization with bistatic MIMO radar, a four-dimensional (4-D) parameter estimation algorithm was proposed in [8] based on centro-symmetric transmit and receive arrays, resorting to the idea of rotation invariance. Further, a mixed-order statistics based method was proposed in [9] to achieve joint estimation of DOA, range and reflectivity for a symmetrical MIMO radar system. However, both algorithms proposed in [8] and [9] are based on the approximated model called Fresnel approximation [10–12]. Although this approximation can simplify the system model, it introduces systematic errors, resulting in reduced estimation accuracy. Using the accurate spherical wavefront model, tensor-based NF source localization algorithms were proposed in [13] and [14], by extracting the angle and range parameters from the estimates of the steering matrices, with improved estimation accuracy as compared to Fresnel approximation adopted in [8, 9]. In [15], the conditional and unconditional Cramer-Rao bounds (CRBs) for NF source parameter estimation are analyzed based on the exact spherical wavefront model for bistatic MIMO radar systems.

The transmit and receive arrays of the MIMO radar system considered above are scalar arrays, which only exploits the spatial information of the FF or NF sources, ignoring the polarization information of signals. On the contrary, vector sensor arrays, such as the electromagnetic vector (EMV) array, can provide not only the angle information of the source, but also the polarization information. Therefore, various direction-finding methods using EMV sensors (EMVS) have been presented [16–20], bringing new insights into the parameter estimation problem in MIMO radar. A two-dimensional (2D)

This work was supported by the Zhejiang Provincial Natural Science Foundation of China under Grant LY23F010003, by the National Natural Science Foundation of China under Grants 62001256 and 62222109, by the Zhejiang Provincial Natural Science Foundation of China (Distinguished Young) under Grant LR20F010001, and the UK Engineering and Physical Sciences Research Council (EPSRC) under grants EP/T517215/1 and EP/V009419/1.

Hua Chen, Weilong Wang, Ye Tian and Gang Wang are with the Faculty of Electrical Engineering and Computer Science, Ningbo University, Ningbo 315211, China. (e-mail: dkchenhua0714@hotmail.com; tianfield@126.com; wanggang@nbu.edu.cn)

Hua Chen is also with the Zhejiang Key Laboratory of Mobile Network Application Technology, Ningbo 315211, P. R. China.

Wei Liu is with the School of Electronic Engineering and Computer Science, Queen Mary University of London, London E1 4NS, UK. (e-mail: wliu.eee@gmail.com; w.liu@sheffield.ac.uk)

DOA estimation method was proposed in [21] for a MIMO radar system equipped with multiple EMV antennas and a single EMV antenna in transmit and receive ends, respectively. As a generalization of the EMVS-MIMO framework in [22], multiple EMV antennas are arranged in both transmitters and receivers, 2D DOD, DOA and associated polarization parameters can be jointly estimated, followed by a pairing procedure. However, it requires eigenvalue decomposition (EVD) and additional pairing operations with a high computational cost, as demonstrated in [23]. Based on rotation invariance and vector cross product, a joint estimation algorithm for 2D DOD/DOA and polarization parameters was proposed for bistatic EMV-MIMO radar based on PARAFAC decomposition [23], which has a more accurate estimation performance, but with reduced complexity compared to [22]. To make full use of spatial diversity of EMV's components, a MIMO radar system composed of spatially spread dipole quints was developed in [24] to obtain the 2D-DOD/DOA and polarization parameters, which is based on non-uniform linear arrays (NLAs) with a spacing larger than half a wavelength, instead of uniform linear arrays (ULAs) in [21–23].

However, the methods proposed in [21–24] are mainly focused on FF sources, while existing NF MIMO radar localization methods in [8, 9, 13, 14] ignore variation of the received signal's amplitude from sensor to sensor; as shown in [25–30], the attenuation of the signal's amplitude is inversely proportional to the source-sensor distance. In addition, each concentered orthogonal loop and dipole (COLD) antenna consists of a pair of spatially co-located but orthogonal magnetic loop and electric dipole [31]. By employing the COLD array, a second-order statistics based near-field source parameter estimation method was proposed in [32]. However, it requires spectral peak search, leading to a high computational complexity. Using the same array as in [32], a search-free algorithm was presented in [33] based on an exact source-sensor spatial propagation geometry. So far, to our best knowledge, no research has been reported on near-field source parameter estimation for bistatic MIMO radar composed of linear COLD arrays at both the transmitter and receiver. To this end, in this paper, an NF source parameter estimation method considering amplitude attenuation is proposed for bistatic MIMO radar composed of a linear COLD array at both the transmitter and receiver. The following is a list of main contributions of the work:

(1) An exact spatial propagation geometry model is adopted in the proposed NF source localization method, which effectively avoids the systematic error caused by the Fresnel approximation and the assumption that the spatial amplitude distribution of the NF signals among different sensors is uniform.

(2) The spatial amplitude ratio is utilized to estimate the parameters in the NF bistatic MIMO radar scenario with COLD arrays, which imposes less restrictions on the configuration of the transmit/receive array sensors; the closed-form estimation results are achieved without spectrum peak search, and they are automatically matched without phase ambiguities.

Notations: $(\cdot)^{-1}$, $(\cdot)^T$, $(\cdot)^+$ and $(\cdot)^H$ represent inverse, transpose, pseudo-inverse, and conjugate transpose, respectively; $\mathbf{I}_p$ stands for the $p\times p$ identity matrix; $\circ$, $\otimes$, $\odot$ and $\oplus$ are the vector outer product, Kronecker product, Khatri-Rao product and Hadamard product, respectively; $\mathbf{1}_p$ represents an all-one $p \times 1$ column vector; $\|\cdot\|_F$ is the Frobenius norm. $abs\{\cdot\}$, $angle\{\cdot\}$, $Re\{\cdot\}$, $diag\{\cdot\}$, $vec\{\cdot\}$ and $unvec\{\cdot\}$ denote the operations of taking absolute value, phase, real part, diagonalization, vectorization and de-vectorization, respectively; $round\{\cdot\}$ gives the nearest integer to its argument $\{\cdot\}$.

II. Signal Model

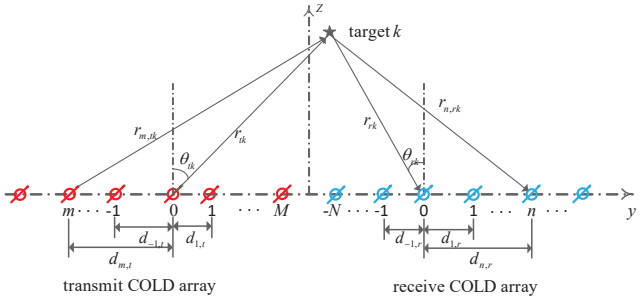

Fig. 1. Geometry of the studied bistatic MIMO radar.

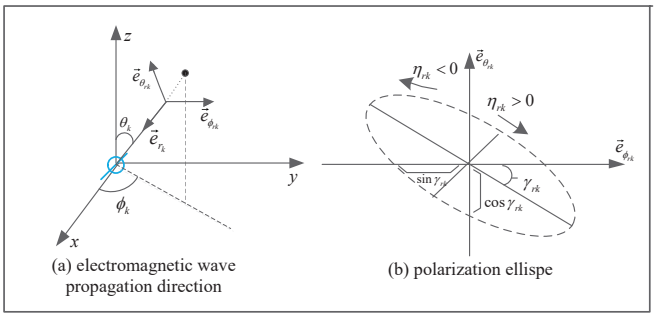

Fig. 2. Illustration of receive polarization parameters [16].

Fig. 1 shows a bistatic MIMO radar system equipped with NLAs of $2M+1$ and $2N+1$ COLD sensors at the transmitter and the receiver, respectively. Assume that K NF targets are located on the $y-z$ plane, parameterized by $(\theta_{t1}, \theta_{r1}, r_{t1}, r_{r1}, \gamma_{t1}, \gamma_{r1}, \eta_{t1}, \eta_{r1}), \cdots, (\theta_{tK}, \theta_{rK}, r_{tK}, r_{rK}, \gamma_{tK}, \gamma_{rK}, \eta_{tK}, \eta_{rK})$, where θ_{tk} and θ_{rk} are the DOD and DOA angles of the k-th target, r_{tk} and r_{rk} are the range from the center of the transmitting array to the k-th target and the range from the k-th target to the center of the receiving array, γ_{tk} and γ_{rk} are the transmit and receive auxiliary polarization angles, η_{tk} and η_{rk} are the transmit and receive polarization phase differences. Taking the receive array as an example, the geometric relationship and details of the auxiliary polarization angles and polarization phase differences are illustrated in Fig. 2.

Note that the target-to-sensor range varies from sensor to sensor, and thus the range between the k-th target and the m-th transmit and n-th receive sensor is denoted as $r_{m,tk}$ and $r_{n,rk}$, respectively, for $m = -M, \cdots, 0, \cdots, M$, and

$n = -N, \cdots, 0, \cdots, N$. Considering the centers of the transmit and receive arrays to be the amplitude and phase reference points, we have $r_{0,tk} = r_{tk}$ and $r_{0,rk} = r_{rk}$. Based on the geometric relationship in Fig. 1, $r_{m,tk}$ and $r_{n,rk}$ can be expressed as

$$r_{m,tk} = \sqrt{r_{tk}^2 + d_{m,t}^2 - 2r_{tk}d_{m,t}\sin(\theta_{tk})} \tag{1}$$

$$r_{n,rk} = \sqrt{r_{rk}^2 + d_{n,r}^2 - 2r_{rk}d_{n,r}\sin(\theta_{rk})} \tag{2}$$

where $d_{m,t}$ and $d_{n,r}$ represent the range between the m-th transmit sensor and the reference transmit sensor, and the range between the n-th receiver sensor and the reference receive sensor, respectively.

Based on the exact target-array propagation geometry, the spatial amplitude-phase factors between the k-th target and the m-th transmit and n-th receive sensor can be expressed as [33]

$$\begin{aligned} a_{m,tk}(\theta_{tk}, r_{tk}) &= b_{m,tk}e^{j(\delta_{m,tk}+\varepsilon_{m,t})} \\ &= \tfrac{r_{tk}}{r_{m,tk}}e^{j\left[\frac{2\pi}{\lambda}(r_{tk}-r_{m,tk})+\varepsilon_{m,t}\right]} \end{aligned} \tag{3}$$

$$\begin{aligned} a_{n,rk}(\theta_{rk}, r_{rk}) &= b_{n,rk}e^{j(\delta_{n,rk}+\varepsilon_{n,r})} \\ &= \tfrac{r_{rk}}{r_{n,rk}}e^{j\left[\frac{2\pi}{\lambda}(r_{rk}-r_{n,rk})+\varepsilon_{n,r}\right]} \end{aligned} \tag{4}$$

where $\varepsilon_{m,t}$ and $\varepsilon_{n,r}$ are the additional phase factors representing unknown phase uncertainty of the m-th transmit and n-th receive sensor, respectively, uniformly distributed in the range of $[0, 2\pi]$; $b_{m,tk} = \frac{r_{tk}}{r_{m,tk}}$ and $b_{n,rk} = \frac{r_{rk}}{r_{n,rk}}$ represent the spatial magnitude attenuation; $\delta_{m,tk}$ and $\delta_{n,rk}$ denote the spatial phase factor due to the propagation delay, and λ is the wavelength of the signals.

Denote the signals transmitted by the transmit array in each pulse period as $\mathbf{S} = [\mathbf{s}_{-M}^T, \cdots, \mathbf{s}_{-1}^T, \mathbf{s}_0^T, \mathbf{s}_1^T, \cdots, \mathbf{s}_M^T] \in \mathbb{C}^{2(2M+1)\times Q}$, where Q is the number of codes, $\mathbf{s}_m = [\mathbf{s}_{m,1}, \mathbf{s}_{m,2}]^T$, and they are received by the receive array after being reflected by the targets. Due to orthogonality of the transmitted signals [7], we have

$$s_{m,i}^H s_{m',j} = \begin{cases} Q, m = m' \ \& \ \ i = j \\ 0, \text{otherwise} \end{cases} \tag{5}$$

for $m, m' = -M, \cdots, M$ and $i, j = 1, 2$. With a non-dispersive propagation environment [7], the received signal matrix at the l-th snapshot can be expressed as

$$\mathbf{X}^{(l)} = \mathbf{Q}_r(\theta_r, r_r, \gamma_r, \eta_r)diag\{\mathbf{b}^{(l)}\}\mathbf{Q}_t^T(\theta_t, r_t, \gamma_t, \eta_t)\mathbf{S} + \mathbf{W}^{(l)}, \tag{6}$$

where $\mathbf{b}^{(l)} = [b_1^{(l)}, b_2^{(l)}, \cdots, b_K^{(l)}]$ contains the reflection coefficients including the Doppler effect and radar cross section (RCS) fading loss. For the Swerling II target model [7, 34], the reflection coefficient of the k-th target at the l-th pulse index can be expressed by $b_k^{(l)} = \beta_k^{(l)}e^{j(l-1)f_k}$, with $\beta_k^{(l)}$ being RCS coefficient varying independently from pulse to pulse and f_k being the Doppler frequency of the k-th target. $\mathbf{W}^{(l)}$ is the white Gaussian noise matrix with zero mean and variance σ_w^2.

$$\begin{aligned} \mathbf{Q}_t(\theta_t, r_t, \gamma_t, \eta_t) = [&\mathbf{q}_t(\theta_{t1}, r_{t1}, \gamma_{t1}, \eta_{t1}), \mathbf{q}_t(\theta_{t2}, r_{t2}, \gamma_{t2}, \eta_{t2}), \\ &\cdots, \mathbf{q}_t(\theta_{tK}, r_{tK}, \gamma_{tK}, \eta_{tK})] \end{aligned} \tag{7}$$

$$\begin{aligned} \mathbf{Q}_r(\theta_r, r_r, \gamma_r, \eta_r) = [&\mathbf{q}_r(\theta_{r1}, r_{r1}, \gamma_{r1}, \eta_{r1}), \mathbf{q}_r(\theta_{r2}, r_{r2}, \gamma_{r2}, \eta_{r2}), \\ &\cdots, \mathbf{q}_r(\theta_{rK}, r_{rK}, \gamma_{rK}, \eta_{rK})] \end{aligned} \tag{8}$$

are the steering matrices of the transmit and receive arrays, respectively, where the steering vector of the transmit array for the k-th target is

$$\mathbf{q}_t(\theta_{tk}, r_{tk}, \gamma_{tk}, \eta_{tk}) = \mathbf{a}_{tk}(\theta_{tk}, r_{tk}) \otimes \mathbf{v}_{tk}(\gamma_{tk}, \eta_{tk}) \tag{9}$$

with $\mathbf{a}_{tk}(\theta_{tk}, r_{tk}) = [a_{-M,tk}(\theta_{tk}, r_{tk}), \cdots a_{0,tk}(\theta_{tk}, r_{tk}), \cdots, a_{M,tk}(\theta_{tk}, r_{tk})]$ being the k-th angle-range-related steering vector at the transmit end, and $\mathbf{v}_{tk}(\gamma_{tk}, \eta_{tk})$ being the k-th polarization vector, denoted as [23]

$$\mathbf{v}_{tk}(\gamma_{tk}, \eta_{tk}) = \begin{pmatrix} \sin\gamma_{tk}e^{j\eta_{tk}} \\ \cos\gamma_{tk} \end{pmatrix} \tag{10}$$

Similarly, the steering vector at the receive end for the k-th target is

$$\mathbf{q}_r(\theta_{rk}, r_{rk}, \gamma_{rk}, \eta_{rk}) = \mathbf{a}_{rk}(\theta_{rk}, r_{rk}) \otimes \mathbf{v}_{rk}(\gamma_{rk}, \eta_{rk}), \tag{11}$$

where $\mathbf{a}_{rk}(\theta_{rk}, r_{rk}) = [a_{-N,rk}(\theta_{rk}, r_{rk}), \cdots a_{0,rk}(\theta_{rk}, r_{rk}), \cdots, a_{N,rk}(\theta_{rk}, r_{rk})]$ is the k-th angle-range-related steering vector and $\mathbf{v}_{rk}(\gamma_{rk}, \eta_{rk})$ is the k-th polarization vector, denoted as [23]

$$\mathbf{v}_{rk}(\gamma_{rk}, \eta_{rk}) = \begin{pmatrix} \sin\gamma_{rk}e^{j\eta_{rk}} \\ \cos\gamma_{rk} \end{pmatrix} \tag{12}$$

After matched filtering (i.e., right-multiplying $\mathbf{X}^{(l)}$ by $\frac{1}{Q}\mathbf{S}^H$), the output vector can be written as

$$\mathbf{Y}^{(l)} = \mathbf{Q}_r(\theta_r, r_r, \gamma_r, \eta_r)diag\{\mathbf{b}^{(l)}\}\mathbf{Q}_t^T(\theta_t, r_t, \gamma_t, \eta_t) + \mathbf{N}^{(l)} \tag{13}$$

where $\mathbf{N}^{(l)} = \frac{1}{Q}\mathbf{W}^{(l)}\mathbf{S}^H$ is the new noise vector after matched filtering.

Performing a vectorization operation on Eq. (13), and taking L snapshots into account, Eq. (13) can be written as

$$\mathbf{Y} = (\mathbf{Q}_t(\theta_t, r_t, \gamma_t, \eta_t) \odot \mathbf{Q}_r(\theta_r, r_r, \gamma_r, \eta_r))\mathbf{B} + \mathbf{N}, \tag{14}$$

where $\mathbf{Q}_t(\theta_t, r_t, \gamma_t, \eta_t) = \mathbf{A}_t(\theta_t, r_t) \odot \mathbf{V}_t(\gamma_t, \eta_t)$, $\mathbf{Q}_r(\theta_r, r_r, \gamma_r, \eta_r) = \mathbf{A}_r(\theta_r, r_r) \odot \mathbf{V}_r(\gamma_r, \eta_r)$,$\mathbf{Y} = [vec(\mathbf{Y}^{(1)}), vec(\mathbf{Y}^{(2)}), \cdots, vec(\mathbf{Y}^{(L)})]$, $\mathbf{B} = [\mathbf{b}^{(1)}, \mathbf{b}^{(2)}, \cdots, \mathbf{b}^{(L)}]$, $\mathbf{N} = [vec(\mathbf{N}^{(1)}), vec(\mathbf{N}^{(2)}), \cdots, vec(\mathbf{N}^{(L)})]$.

III. THE PROPOSED ALGORITHM

A. Trilinear decomposition

According to Eq. (14), $\mathbf{Y}$ can be rearranged into a fifth-order tensor as follows

$$\begin{aligned} \boldsymbol{\mathcal{Y}} &= \sum_{k=1}^{K} \mathbf{a}_t \circ \mathbf{v}_t \circ \mathbf{a}_r \circ \mathbf{v}_r \circ \mathbf{b} + \tilde{\boldsymbol{\mathcal{N}}} \\ &= \boldsymbol{\mathcal{G}}_{5,K\times 1}\mathbf{A}_{t\times 2}\mathbf{V}_{t\times 3}\mathbf{A}_{r\times 4}\mathbf{V}_{r\times 5}\mathbf{B} + \tilde{\boldsymbol{\mathcal{N}}} \end{aligned} \tag{15}$$

where $\boldsymbol{\mathcal{G}}_{5,K\times 1}$ is a $K \times K \times K \times K \times K$ identity tensor, i.e., its (k, k, k, k, k)-th element is one, and zeros elsewhere. $\tilde{\boldsymbol{\mathcal{N}}}$ is the tensor form of $\mathbf{N}$.

Then, in order to obtain estimates of multiple factor matrices in Eq. (15), a direct method is to exploit the pentalinear

alternating least squares (ALS) technique [35], which tries to optimize

$$\min_{\mathbf{A}_t,\mathbf{V}_t,\mathbf{A}_r,\mathbf{V}_r,\mathbf{B}} \|\mathcal{Y} - \mathcal{G}_{5,K\times 1}\mathbf{A}_{t\times 2}\mathbf{V}_{t\times 3}\mathbf{A}_{r\times 4}\mathbf{V}_{r\times 5}\mathbf{B}\|_F \quad (16)$$

However, ALS suffers from a slow convergence speed, so the COMplex parallel FACtor analysis (COMFAC) algorithm is employed to speed up the process in this work [36]. Further, in order to apply the COMFAC algorithm, we need to compress $\mathcal{Y}$ into a third-order tensor $\mathcal{Z}$.

Definition 1 (Generalized Tensorization of a PARAFAC model [23]): For an Nth-order tensor $\mathcal{R}$ with rank-K, given by $\mathcal{R} = \mathcal{G}_{N,K\times 1}(\mathbf{A}_1)_{\times 2}(\mathbf{A}_2)_{\times 3}\cdots(\mathbf{A}_{N-1})_{\times N}(\mathbf{A}_N)$, let the order sets $\mathbb{Q}_j = \{o_{j,1}, o_{j,2}, \cdots, o_{j,M}\}$ for $j = 1, 2, \cdots, J$ be a partition of the dimensions $\mathbb{Q} = \{1, 2, \cdots, N\}$, and then the generalized tensorization of $\mathcal{R}$ is denoted by a new tensor $\mathcal{R}_{\mathbb{Q}_1,\mathbb{Q}_2,\cdots,\mathbb{Q}_J}$ with

$$\mathcal{R}_{\mathbb{Q}_1,\mathbb{Q}_2,\cdots,\mathbb{Q}_J} = \mathcal{G}_{N,\times 1}(\mathbf{B}_1)_{\times 2}(\mathbf{B}_2)_{\times 3}\cdots(\mathbf{B}_{J-1})_{\times J}(\mathbf{B}_J) \quad (17)$$

where $\mathbf{B}_J = \mathbf{A}_{o_{j,1}} \odot \mathbf{A}_{o_{j,2}} \odot \mathbf{A}_{o,M_j}$.

According to **Definition 1**, with $\mathbb{O}_1 = \{1, 2\}, \mathbb{O}_2 = \{3, 4\}$, and $\mathbb{O}_3 = \{5\}$, $\mathcal{Y}$ can be rearranged into a third-order tensor as follows

$$\mathcal{Z} = \mathcal{G}_{3,K\times 1}\mathbf{Q}_{t\times 2}\mathbf{Q}_{r\times 3}\mathbf{B} + \mathcal{N}, \quad (18)$$

where $\mathcal{G}_{3,K\times 1}$ is a $K \times K \times K$ identity tensor, and $\mathcal{N}$ is the corresponding tensor form.

Definition 2 (PARAFAC decomposition [23]): For an Nth-order model of **Definition 1**, it can be expressed in a matrix form as

$$[\mathcal{R}]_n = \mathbf{A}_n[\mathbf{A}_N \odot \cdots \mathbf{A}_{n+1} \odot \mathbf{A}_{n-1}\cdots\mathbf{A}_1]^T \quad (19)$$

Taking a third-order tensor $\mathcal{R} \in \mathbb{C}^{I\times J\times K}$ in N factors as an example, its PARAFAC decomposition can be represented in Fig. 3.

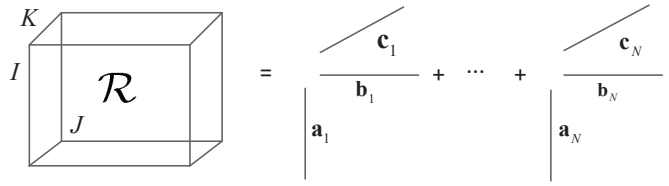

Fig. 3. Schematic representation of PARAFAC decomposition.

Then, according to **Definition 2**, $\mathcal{Z}$ can be unfolded in matrix form as

$$[\mathcal{Z}]_{(1)} = (\mathbf{Q}_r \odot \mathbf{B})\mathbf{Q}_t^T \quad (20)$$

$$[\mathcal{Z}]_{(2)} = (\mathbf{B} \odot \mathbf{Q}_t)\mathbf{Q}_r^T \quad (21)$$

$$[\mathcal{Z}]_{(3)} = (\mathbf{Q}_t \odot \mathbf{Q}_r)\mathbf{B}^T. \quad (22)$$

Let $\hat{\mathcal{Z}}$ represent the estimate of $\mathcal{Z}$, and define $\hat{\mathbf{Z}}_n = [\hat{\mathcal{Z}}]_{(n)}, (n = 1, 2, 3)$. The factor matrices $\mathbf{Q}_t, \mathbf{Q}_r, \mathbf{B}$ can be obtained by the following joint optimizations

$$\min_{\mathbf{Q}_t,\mathbf{Q}_r,\mathbf{B}} \| \hat{\mathbf{Z}}_1 - (\mathbf{Q}_r \odot \mathbf{B})\mathbf{Q}_t^T\|_F \quad (23)$$

$$\min_{\mathbf{Q}_t,\mathbf{Q}_r,\mathbf{B}} \| \hat{\mathbf{Z}}_2 - (\mathbf{B} \odot \mathbf{Q}_t)\mathbf{Q}_r^T\|_F \quad (24)$$

$$\min_{\mathbf{Q}_t,\mathbf{Q}_r,\mathbf{B}} \| \hat{\mathbf{Z}}_3 - (\mathbf{Q}_t \odot \mathbf{Q}_r)\mathbf{B}^T\|_F. \quad (25)$$

The optimization problem of Eqs. (23)-(25) is generally solved through the trilinear alternating least squares (TALS) method [37], the basic idea of which is to assume that any two of $\mathbf{Q}_t, \mathbf{Q}_r$ and $\mathbf{B}$ are known during each iteration process, and then update the remaining one based on the least squares (LS) method until the algorithm converges. Therefore, according to Eq. (23), if $\mathbf{Q}_r$ and $\mathbf{B}$ are known, the LS update of $\mathbf{Q}_t$ can be represented as

$$\hat{\mathbf{Q}}_t^T = (\mathbf{Q}_r \odot \mathbf{B})^+\hat{\mathbf{Z}}_1 \quad (26)$$

Likewise, according to Eq. (24), if $\mathbf{B}$ and $\mathbf{Q}_t$ are obtained, the LS update of $\mathbf{Q}_r$ can be denoted as

$$\hat{\mathbf{Q}}_r^T = (\mathbf{B} \odot \mathbf{Q}_t)^+\hat{\mathbf{Z}}_2 \quad (27)$$

Similarly, according to Eq. (25), if $\mathbf{Q}_t$ and $\mathbf{Q}_r$ are known, the LS solution of $\mathbf{B}$ is updated as

$$\hat{\mathbf{B}}^T = (\mathbf{Q}_t \odot \mathbf{Q}_r)^+\hat{\mathbf{Z}}_3. \quad (28)$$

In the TALS method, $\mathbf{Q}_t$, $\mathbf{Q}_r$ and $\mathbf{B}$ are updated sequentially according to Eqs. (26)-(28), and the process is repeated until convergence. Finally, the estimates of $\mathbf{Q}_t$, $\mathbf{Q}_r$ and $\mathbf{B}$ can be obtained. Since the convergence speed of TALS is slow, the COMFAC algorithm is employed to speed up the process in this work [36].

Let the Kruskal ranks of $\mathbf{Q}_t$, $\mathbf{Q}_r$ and $\mathbf{B}$ be $k_{\mathbf{Q}_t}$, $k_{\mathbf{Q}_r}$, and $k_{\mathbf{B}}$, respectively. According to the Kruskal's theorem [7, 23], if

$$k_{\mathbf{Q}_t} + k_{\mathbf{Q}_r} + k_{\mathbf{B}} \geq 2K + 3, \quad (29)$$

then the estimates of $\hat{\mathbf{Q}}_t$, $\hat{\mathbf{Q}}_r$ and $\hat{\mathbf{B}}$ are unique up to some permutation and scaling of the columns. In other words, the estimates of $\hat{\mathbf{Q}}_t$, $\hat{\mathbf{Q}}_r$ and $\hat{\mathbf{B}}$ satisfy

$$\hat{\mathbf{Q}}_t = \mathbf{Q}_t\mathbf{\Pi}\mathbf{\Delta}_1 + \mathbf{N}_1 \quad (30)$$

$$\hat{\mathbf{Q}}_r = \mathbf{Q}_r\mathbf{\Pi}\mathbf{\Delta}_2 + \mathbf{N}_2 \quad (31)$$

$$\hat{\mathbf{B}} = \mathbf{B}\mathbf{\Pi}\mathbf{\Delta}_3 + \mathbf{N}_3 \quad (32)$$

where $\mathbf{\Pi}$ is a permutation matrix, $\mathbf{\Delta}_1$, $\mathbf{\Delta}_2$ and $\mathbf{\Delta}_3$ represent scaling effects, which are $K\times K$ real-valued diagonal matrices, satisfying $\mathbf{\Delta}_1\mathbf{\Delta}_2\mathbf{\Delta}_3 = \mathbf{I}_K$, and $\mathbf{N}_1$, $\mathbf{N}_2$ and $\mathbf{N}_3$ are the fitting error matrices.

B. DOD and TPA Estimation

To proceed, construct the following transformation matrix

$$\mathbf{C}_t = \underbrace{\begin{pmatrix} 1 & 0 & & & & & \\ & & 1 & 0 & & & \\ & & & & \ddots & & \\ & & & & & 1 & 0 \\ 0 & 1 & & & & & \\ & & 0 & 1 & & & \\ & & & & \ddots & & \\ & & & & & 0 & 1 \end{pmatrix}}_{2M+1} \begin{matrix} \left.\begin{matrix} \\ \\ \\ \\ \end{matrix}\right\} 2M+1 \\ \left.\begin{matrix} \\ \\ \\ \\ \end{matrix}\right\} 2M+1 \end{matrix}. \quad (33)$$

Then, ignoring the error term in Eq. (30), we can obtain

$$\mathbf{C}_t\hat{\mathbf{Q}}_t \approx \mathbf{C}_t\mathbf{Q}_t\mathbf{\Pi}\mathbf{\Delta}_1. \quad (34)$$

Since $\mathbf{Q}_t = \mathbf{A}_t \odot \mathbf{V}_t$, Eq. (34) can be rewritten as

$$\mathbf{C}_t\hat{\mathbf{Q}}_t \approx \begin{pmatrix} \mathbf{A}_t\mathbf{\Phi}_{t1} \\ \mathbf{A}_t\mathbf{\Phi}_{t2} \end{pmatrix} \mathbf{\Pi}\mathbf{\Delta}_1, \quad (35)$$

where $\mathbf{\Phi}_{t1} = diag(\sin\gamma_{t1}e^{j\eta_{t1}}, \cdots, \sin\gamma_{tK}e^{j\eta_{tK}})$, $\mathbf{\Phi}_{t2} = diag(\cos\gamma_{t1}, \cdots, \cos\gamma_{tK})$,. Let $\mathbf{D}_{t1} = \mathbf{A}_t\mathbf{\Phi}_{t1}\mathbf{\Pi}\mathbf{\Delta}_1$ and $\mathbf{D}_{t2} = \mathbf{A}_t\mathbf{\Phi}_{t2}\mathbf{\Pi}\mathbf{\Delta}_1$ with $\mathbf{\Pi}\mathbf{\Delta}_1 = \mathbf{\Delta}_1\mathbf{\Pi}^{-1}$ [23], and we have

$$\mathbf{D}_{t1}^{+}\mathbf{D}_{t2} = \mathbf{\Pi}(\mathbf{\Phi}_{t1}^{-1}\mathbf{\Phi}_{t2})\mathbf{\Pi}^{-1} \quad (36)$$

where $\mathbf{\Phi}_{t1}^{-1}\mathbf{\Phi}_{t2} = diag(\cot\gamma_{t1}e^{-j\eta_{t1}}, \cdots, \cot\gamma_{tK}e^{-j\eta_{tK}})$.

Perform eigenvalue decomposition on $\mathbf{D}_{t1}^{+}\mathbf{D}_{t2}$ to obtain its eigenvalues as $\mathbf{\Psi} = diag(\tau_{t1}, \cdots \tau_{tK})$, and the corresponding eigenvectors as $\mathbf{P} = [\mathbf{o}_{t1}, \cdots, \mathbf{o}_{tK}]$. As a result, the transmit polarization parameters can be estimated through

$$\hat{\eta}_{tk} = -angle(\tau_{tk}) \quad (37)$$

$$\hat{\gamma}_{tk} = cot^{-1}(abs(\tau_{tk})). \quad (38)$$

The estimate of the permutation matrix $\mathbf{\Pi}$ can be expressed as

$$\hat{\mathbf{\Pi}} = round\{\mathrm{Re}(\mathbf{P})\}. \quad (39)$$

With the estimates of η_{tk} and γ_{tk}, we can calculate the estimate of $\mathbf{v}_{tk}$ via

$$\hat{\mathbf{v}}_{tk} = \begin{pmatrix} \sin\hat{\gamma}_{tk}e^{j\hat{\eta}_{tk}} \\ \cos\hat{\gamma}_{tk} \end{pmatrix} \quad (40)$$

Since $\mathbf{Q}_t = [\mathbf{q}_{t1}, \cdots, \mathbf{q}_{tK}] = \mathbf{A}_t \odot \mathbf{V}_t = [vec(\mathbf{v}_{t1}\mathbf{a}_{t1}^T), \cdots, vec(\mathbf{v}_{tK}\mathbf{a}_{tK}^T)]$, $\mathbf{a}_{tk}$ can be estimated as

$$\hat{\mathbf{a}}_{tk} = [\hat{\mathbf{v}}_{tk}^{+}unvec(\hat{\mathbf{q}}_{tk})]^T. \quad (41)$$

Note that $\hat{\mathbf{a}}_{tk}$ is correct up to an unknown complex-valued scalar, and thus the scaling ambiguity of the estimate $\hat{\mathbf{a}}_{tk}$ can be easily solved by the normalization operation, i.e., normalizing each element $\hat{a}_{m,tk}(m \neq 0)$ in $\hat{\mathbf{a}}_{tk}$ with respect to the reference element $\hat{a}_{0,tk}$. Then, for any $m \neq 0$, we can obtain

$$\hat{b}_{m,tk} = \frac{\hat{r}_{tk}}{\hat{r}_{m,tk}} = \frac{\hat{r}_{tk}}{\sqrt{\hat{r}_{tk}^2 + d_{m,t}^2 - 2\hat{r}_{tk}d_{m,t}\sin(\hat{\theta}_{tk})}}. \quad (42)$$

Rearranging Eq. (42), we have

$$(1-\hat{b}_{m,tk}^2)\hat{r}_{tk}^2 + 2\hat{b}_{m,tk}^2 d_{m,t}\hat{r}_{tk}\sin(\hat{\theta}_{tk}) = \hat{b}_{m,tk}^2 d_{m,t}^2. \quad (43)$$

This is an overdetermined system of linear equations in $\hat{r}_{tk}^2$ and $\hat{r}_{tk}\sin(\hat{\theta}_{tk})$, which can be solved by the total least squares method. Let $[v_{1k}, v_{2k}, v_{3k}]$ denote the right singular vector corresponding to the smallest singular value of the coefficient matrix of the overdetermined system of equations in (43) with $m = -M, \cdots -1, 1, \cdots, M$. Then, r_{tk} and θ_{tk} can be estimated via

$$\hat{r}_{tk} = sqrt(v_{1k}/v_{3k}) \quad (44)$$

$$\hat{\theta}_{tk} = \sin^{-1}(v_{2k}/\hat{r}_{tk}). \quad (45)$$

C. DOA and RPA Estimation

Similar to Eq. (33), let

$$\mathbf{C}_r = \underbrace{\begin{pmatrix} 1 & 0 & & & & & \\ & & 1 & 0 & & & \\ & & & & \ddots & & \\ & & & & & 1 & 0 \\ 0 & 1 & & & & & \\ & & 0 & 1 & & & \\ & & & & \ddots & & \\ & & & & & 0 & 1 \end{pmatrix}}_{2N+1} \begin{matrix} \left.\begin{matrix} \\ \\ \\ \\ \end{matrix}\right\} 2N+1 \\ \left.\begin{matrix} \\ \\ \\ \\ \end{matrix}\right\} 2N+1 \end{matrix}. \quad (46)$$

Then, ignoring the error term in Eq. (31), we have

$$\mathbf{C}_r\hat{\mathbf{Q}}_r \approx \mathbf{C}_r\mathbf{Q}_r\mathbf{\Pi}\mathbf{\Delta}_2. \quad (47)$$

With $\mathbf{Q}_r = \mathbf{A}_r \odot \mathbf{V}_r$, we further have

$$\mathbf{C}_r\hat{\mathbf{Q}}_r \approx \begin{pmatrix} \mathbf{A}_r\mathbf{\Phi}_{r1} \\ \mathbf{A}_r\mathbf{\Phi}_{r2}, \end{pmatrix} \mathbf{\Pi}\mathbf{\Delta}_2 \quad (48)$$

where $\mathbf{\Phi}_{r1} = diag(\sin\gamma_{r1}e^{j\eta_{r1}}, \cdots, \sin\gamma_{rK}e^{j\eta_{rK}})$, and $\mathbf{\Phi}_{r2} = diag(\cos\gamma_{r1}, \cdots, \cos\gamma_{rK})$.

Let $\mathbf{D}_{r1} = \mathbf{A}_r\mathbf{\Phi}_{r1}\mathbf{\Pi}\mathbf{\Delta}_2$ and $\mathbf{D}_{r2} = \mathbf{A}_r\mathbf{\Phi}_{r2}\mathbf{\Pi}\mathbf{\Delta}_2$, and then,

$$\mathbf{D}_{r1}^{+}\mathbf{D}_{r2} = \mathbf{\Pi}(\mathbf{\Phi}_{r1}^{-1}\mathbf{\Phi}_{r2})\mathbf{\Pi}^{-1}, \quad (49)$$

where $\mathbf{\Phi}_{r1}^{-1}\mathbf{\Phi}_{r2} = diag(\cot\gamma_{r1}e^{-j\eta_{r1}}, \cdots, \cot\gamma_{rK}e^{-j\eta_{rK}})$. From Eq. (36) and Eq. (49), it can be seen that $\mathbf{D}_{t1}^{+}\mathbf{D}_{t2}$ and $\mathbf{D}_{r1}^{+}\mathbf{D}_{r2}$ have the same eigenvectors $\mathbf{\Pi}$. Thus, the estimate of $\mathbf{\Phi}_{r1}^{-1}\mathbf{\Phi}_{r2}$ can be directly obtained as

$$\mathbf{T} = \hat{\mathbf{\Pi}}^{-1}\mathbf{D}_{r1}^{+}\mathbf{D}_{r2}\hat{\mathbf{\Pi}}. \quad (50)$$

Then, the receive polarization parameters can be estimated via

$$\hat{\eta}_{rk} = -angle(\mathbf{T}(k)) \quad (51)$$

$$\hat{\gamma}_{rk} = cot^{-1}(abs(\mathbf{T}(k)). \quad (52)$$

Performing operations similar to Eqs. (39)-(45), finally we obtain the estimates $\hat{r}_{rk}$ and $\hat{\theta}_{rk}$.

D. Unknown Phase Uncertainty Estimation

As mentioned before, only the spatial amplitude ratio of the array steering vector is exploited for the angle and range parameters in both transmit and receive arrays, not the phase, which is subject to additional unknown phase uncertainty. With the estimates $\hat{r}_{tk}$, $\hat{\theta}_{tk}$, $\hat{r}_{rk}$ and $\hat{\theta}_{rk}$, the array steering vectors without phase error can be reconstructed. By denoting the phase errors of transmitter and receiver as $\varepsilon_{m,t}$ and $\varepsilon_{n,t}$, we can estimate $\varepsilon_{m,t}$ and $\varepsilon_{n,t}$ through the follow phase-taking and averaging operations,

$$\hat{\varepsilon}_{m,t} = \frac{1}{K}\sum_{k=1}^{K} angle\left(\frac{\hat{a}_{m,tk}\left(\theta_{tk}, r_{tk}\right)}{\bar{a}_{m,tk}\left(\hat{\theta}_{tk}, \hat{r}_{tk}\right)}\right) \tag{53}$$

and

$$\hat{\varepsilon}_{n,r} = \frac{1}{K}\sum_{k=1}^{K} angle\left(\frac{\hat{a}_{n,rk}\left(\theta_{rk}, r_{rk}\right)}{\bar{a}_{n,rk}\left(\hat{\theta}_{rk}, \hat{r}_{rk}\right)}\right) \tag{54}$$

where $\bar{a}_{m,tk}\left(\hat{\theta}_{tk}, \hat{r}_{tk}\right) = \frac{\hat{r}_{tk}}{\hat{r}_{m,tk}} e^{j\left[\frac{2\pi}{\lambda}\left(\hat{r}_{tk}-\hat{r}_{m,tk}\right)\right]}$ and $\bar{a}_{n,rk}\left(\hat{\theta}_{rk}, \hat{r}_{rk}\right) = \frac{\hat{r}_{rk}}{\hat{r}_{n,rk}} e^{j\left[\frac{2\pi}{\lambda}\left(\hat{r}_{rk}-\hat{r}_{n,rk}\right)\right]}$.

Remark 1: The motivation for using the amplitude information is that, as pointed out in [25], amplitude attenuation cannot be ignored for the NF propagation model. As amplitude attenuation is related to both angle and range parameters, it provides useful information for parameter estimation usually achieved from spatial phase information. In addition, due to the existence of phase error in the signal model, it is difficult to estimate DOD, DOA, RFTT, and RFTR from the spatial phase information directly. Therefore, in this work, the spatial amplitude information is exploited to obtain the estimates of DOD, DOA, RFTT, and RFTR, while the spatial phase information is exploited for estimation of phase errors.

IV. Algorithm analysis

A. Cramer-Rao bound (CRB)

In this section, the deterministic Cramer-Rao bound (CRB) is derived for the studied bistatic MIMO system in which both the transmitter and the receiver are equipped with COLD sensor arrays.

First, define a real-valued vector of unknown parameters as $\boldsymbol{\Theta} = [\boldsymbol{\theta}_t^T, \boldsymbol{\theta}_r^T, \mathbf{r}_t^T, \mathbf{r}_r^T, \boldsymbol{\gamma}_t^T, \boldsymbol{\gamma}_r^T, \boldsymbol{\eta}_t^T, \boldsymbol{\eta}_r^T]^T$ with $\boldsymbol{\theta}_t = [\theta_{t1}, \theta_{t2}, \cdots, \theta_{tK}]^T$, $\boldsymbol{\theta}_r = [\theta_{r1}, \theta_{r2}, \cdots, \theta_{rK}]^T$, $\mathbf{r}_t = [r_{t1}, r_{t2}, \cdots, r_{tK}]^T$, $\mathbf{r}_r = [r_{r1}, r_{r2}, \cdots, r_{rK}]^T$, $\boldsymbol{\gamma}_t = [\gamma_{t1}, \gamma_{t2}, \cdots, \gamma_{tK}]^T$, $\boldsymbol{\gamma}_r = [\gamma_{r1}, \gamma_{r2}, \cdots, \gamma_{rK}]^T$, $\boldsymbol{\eta}_t = [\eta_{t1}, \eta_{t2}, \cdots, \eta_{tK}]^T$ and $\boldsymbol{\eta}_r = [\eta_{r1}, \eta_{r2}, \cdots, \eta_{rK}]^T$. Then, the (p,q)th entry of the $8K \times 8K$ CRB matrix for the parameters in $\boldsymbol{\Theta}$ is given by

$$[CRB^{-1}(\boldsymbol{\Theta})]_{p,q} = \frac{2L}{\sigma_n^2} Re\left\{\frac{\partial \mathbf{Q}^H}{\partial \boldsymbol{\Theta}_p}\mathbf{P}_{\mathbf{Q}}^{\perp}\frac{\partial \mathbf{Q}}{\partial \boldsymbol{\Theta}_q}\mathbf{R}_B\right\}, \tag{55}$$

where $\mathbf{Q} = \mathbf{Q}_t \odot \mathbf{Q}_r$, $\mathbf{P}_{\mathbf{D}}^{\perp} = \mathbf{I}_{4(2M+1)(2N+1)} - \mathbf{Q}(\mathbf{Q}^H\mathbf{Q})^{-1}\mathbf{Q}^H$, and $\mathbf{R}_B = \frac{1}{L}\mathbf{B}^H\mathbf{B}$.

Define

$$\tilde{\mathbf{Q}} = [\mathbf{Q}_{\theta_t}, \mathbf{Q}_{\theta_r}, \mathbf{Q}_{r_t}, \mathbf{Q}_{r_r}, \mathbf{Q}_{\gamma_t}, \mathbf{Q}_{\gamma_r}, \mathbf{Q}_{\eta_t}, \mathbf{Q}_{\eta_r}] \tag{56}$$

with $\mathbf{Q}_{\theta_t} = \left[\frac{\partial \mathbf{Q}}{\partial \theta_{t1}}, \cdots, \frac{\partial \mathbf{Q}}{\partial \theta_{tK}}\right]$, $\mathbf{Q}_{\theta_r} = \left[\frac{\partial \mathbf{Q}}{\partial \theta_{r1}}, \cdots, \frac{\partial \mathbf{Q}}{\partial \theta_{rK}}\right]$, $\mathbf{Q}_{r_t} = \left[\frac{\partial \mathbf{Q}}{\partial r_{t1}}, \cdots, \frac{\partial \mathbf{Q}}{\partial r_{tK}}\right]$, $\mathbf{Q}_{r_r} = \left[\frac{\partial \mathbf{Q}}{\partial r_{r1}}, \cdots, \frac{\partial \mathbf{Q}}{\partial r_{rK}}\right]$, $\mathbf{Q}_{\gamma_t} = \left[\frac{\partial \mathbf{Q}}{\partial \gamma_{t1}}, \cdots, \frac{\partial \mathbf{Q}}{\partial \gamma_{tK}}\right]$, $\mathbf{Q}_{\gamma_r} = \left[\frac{\partial \mathbf{Q}}{\partial \gamma_{r1}}, \cdots, \frac{\partial \mathbf{Q}}{\partial \gamma_{rK}}\right]$, $\mathbf{Q}_{\eta_t} = \left[\frac{\partial \mathbf{Q}}{\partial \eta_{t1}}, \cdots, \frac{\partial \mathbf{Q}}{\partial \eta_{tK}}\right]$ and $\mathbf{Q}_{\eta_r} = \left[\frac{\partial \mathbf{Q}}{\partial \eta_{r1}}, \cdots, \frac{\partial \mathbf{Q}}{\partial \eta_{rK}}\right]$. After a series of simplifications, the closed-form expression for the CRB is given by

$$CRB(\boldsymbol{\Theta}) = \frac{\sigma_n^2}{2L}\left\{Re\left[\left(\tilde{\mathbf{Q}}^H\mathbf{P}_{\mathbf{Q}}^{\perp}\tilde{\mathbf{Q}}\right) \oplus \left(\mathbf{1}_8 \otimes \mathbf{1}_8^T \otimes \mathbf{R}_B^T\right)\right]\right\}^{-1} \tag{57}$$

B. The maximum number of identifiable targets

Assume that the maximum number of identifiable targets is K. The value of K depends on the condition of the uniqueness of the PARAFAC decomposition, which can be determined by the Kruskal's theorem. It can be found that $\max(k_{\mathbf{Q}_t}) = 2(2M+1)$, $\max(k_{\mathbf{Q}_r}) = 2(2N+1)$, and $\max\{k_{\mathbf{B}}\} = L$. As a result, the value of K can be obtained as

$$K = \frac{2(2M+1) + 2(2N+1) + L - 3}{2}. \tag{58}$$

Besides, the value of K relies also on the rotation invariant relationship in Eq. (36) and Eq. (49), satisfying the following constraints

$$\begin{cases} K \le 2M+1 \\ K \le 2N+1 \end{cases}. \tag{59}$$

According to Eq. (58) and Eq. (59), if $M > N$, then $K = 2N+1$; if $M < N$, $K = 2M+1$. Therefore, the maximum number of identifiable targets is

$$K = \min\{2M+1, 2N+1\}. \tag{60}$$

C. Computational Complexity

In this subsection, the computational complexity of the proposed method is analyzed by considering the number of multiplications required in PARAFAC decomposition and eigenvalue decomposition. Specifically, we analyze the following major computations:

(1) $\hat{\mathbf{Q}}_t$, $\hat{\mathbf{Q}}_r$ and $\hat{\mathbf{B}}$ can be obtained via PARAFAC decomposition.

(2) Construct $\mathbf{C}_t$, get $\mathbf{D}_{t1}^{+}\mathbf{D}_{t2}$, and then perform eigenvalue decomposition to it.

(3) Construct $\mathbf{C}_r$ to get $\mathbf{D}_{r1}^{+}\mathbf{D}_{r2}$, and then obtain $\mathbf{T}$ via Eq. (50).

The required number of multiplications for PARAFAC decomposition is $2(2M+1)K^2 + 2(2N+1)K^2 + LK^2$. The number of multiplication operations involved in the eigenvalue decomposition of $\mathbf{D}_{t1}^{+}\mathbf{D}_{t2}$ is $2K(2M+1)^2 + (2M+1)K^2 + K^3$. Besides, the number of multiplications needed in eigenvalue decomposition of $\mathbf{D}_{r1}^{+}\mathbf{D}_{r2}$ and calculating $\mathbf{T}$ is $2K(2N+1)^2 + K^2(2N+1) + 2K^3$.

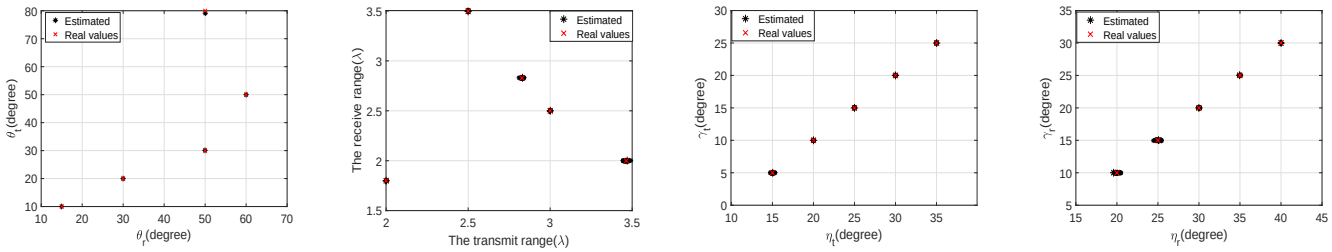

(a) DOD and DOA estimation. (b) RFTR and RFTT estimation. (c) 2-D TPA estimation. (d) 2-D RPA estimation

Fig. 4. Scatter results of the proposed method.

V. Simulation Results

In this section, we evaluate the performance of the proposed method by Monte Carlo simulations. Unless otherwise stated, the number of snapshots is set to 1000. The following scenarios are considered:

Scenario 1: $K = 5$, with their parameters $(\theta_{tk}, \theta_{rk}, r_{tk}, r_{rk}, \gamma_{tk}, \gamma_{rk}, \eta_{tk}, \eta_{rk})$ being $\left(30^\circ, 50^\circ, 2\sqrt{3}\lambda, 2\lambda, 5^\circ, 15^\circ, 10^\circ, 10^\circ\right)$, $\left(80^\circ, 50^\circ, 2\sqrt{2}\lambda, 2\sqrt{2}\lambda, 10^\circ, 20^\circ, 15^\circ, 25^\circ\right)$, $(50^\circ, 60^\circ, 2\lambda, 1.8\lambda, 15^\circ, 25^\circ, 20^\circ, 30^\circ)$, $(20^\circ, 30^\circ, 3\lambda, 2.5\lambda, 20^\circ, 30^\circ, 25^\circ, 35^\circ)$ and $(10^\circ, 15^\circ, 2.5\lambda, 3.5\lambda, 25^\circ, 35^\circ, 30^\circ, 40^\circ)$. $M = N = 2$, with $d_t = [-0.8, -0.3, 0, 0.3, 0.8]\lambda$, $d_r = [-0.8, -0.3, 0, 0.3, 0.8]\lambda$, $\varepsilon_{m,t} = [40^\circ, -20^\circ, 0^\circ, 60^\circ, 80^\circ]$, $\varepsilon_{n,r} = [30^\circ, -10^\circ, 0^\circ, 20^\circ, 50^\circ]$.

Scenario 2: $K = 2$, with their parameters $(\theta_{tk}, \theta_{rk}, r_{tk}, r_{rk}, \gamma_{tk}, \gamma_{rk}, \eta_{tk}, \eta_{rk})$ being $(30^\circ, 60^\circ, 2\sqrt{3}\lambda, 3.5\lambda, 10^\circ, 42^\circ, 50^\circ, 17^\circ)$ and $(45^\circ, 45^\circ, 4\lambda, 4\lambda, 22^\circ, 33^\circ, 55^\circ, 28^\circ)$. $M = N = 4$, with $d_t = [-1.5, -1.2, -0.8, -0.3, 0, 0.3, 0.8, 1.2, 1.5]\lambda$, $d_r = [-1, -0.8, -0.5, -0.3, 0, 0.3, 0.5, 0.8, 1]\lambda$, $\varepsilon_{m,t} = [10^\circ, 30^\circ, 40^\circ, -20^\circ, 0^\circ, 60^\circ, 80^\circ, 25^\circ, 55^\circ]$, $\varepsilon_{n,r} = [5^\circ, -60^\circ, 30^\circ, -10^\circ, 0^\circ, 20^\circ, 50^\circ, 22^\circ, 56^\circ]$.

Scenario 3: $K = 2$, with their parameters $(\theta_{tk}, \theta_{rk}, r_{tk}, r_{rk}, \gamma_{tk}, \gamma_{rk}, \eta_{tk}, \eta_{rk})$ being $(60^\circ, 30^\circ, 2\lambda, 2\sqrt{3}\lambda, 10^\circ, 42^\circ, 50^\circ, 17^\circ)$ and $(45^\circ, 45^\circ, 3\lambda, 3\lambda, 22^\circ, 33^\circ, 55^\circ, 28^\circ)$. $M = N = 4$, with $d_t = [-1, -0.75, -0.5, -0.25, 0, 0.25, 0.5, 0.75, 1]\,\lambda$, $d_r = [-1, -0.75, -0.5, -0.25, 0, 0.25, 0.5, 0.75, 1]\,\lambda$, $\varepsilon_{m,t} = [10^\circ, 30^\circ, 40^\circ, -20^\circ, 0^\circ, 60^\circ, 80^\circ, 25^\circ, 55^\circ]$, $\varepsilon_{n,r} = [5^\circ, -60^\circ, 30^\circ, -10^\circ, 0^\circ, 20^\circ, 50^\circ, 22^\circ, 56^\circ]$.

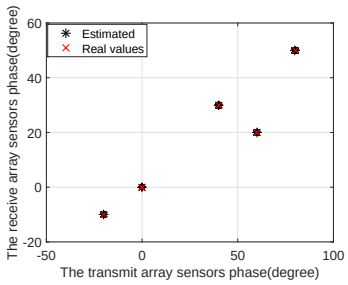

Fig. 5. Scatter results of sensor phase uncertainties.

Scenario 4: $K = 2$, with their parameters $(\theta_{tk}, \theta_{rk}, r_{tk}, r_{rk}, \gamma_{tk}, \gamma_{rk}, \eta_{tk}, \eta_{rk})$ being $(60^\circ, 30^\circ, 2\lambda, 2\sqrt{3}\lambda, 10^\circ, 42^\circ, 50^\circ, 17^\circ)$ and $(45^\circ, 45^\circ, 3\lambda, 3\lambda, 22^\circ, 33^\circ, 55^\circ, 28^\circ)$. $N = 4$ with $d_r = [-1, -0.75, -0.5, -0.25, 0, 0.25, 0.5, 0.75, 1]\,\lambda$ and $\varepsilon_{n,r} = [5^\circ, -60^\circ, 30^\circ, -10^\circ, 0^\circ, 20^\circ, 50^\circ, 22^\circ, 56^\circ]$. Set two cases for the number of transmit elements for comparison: $M = 2$ with $d_t = [-1, -0.5, 0, 0.5, 1]\,\lambda$ and $\varepsilon_{m,t} = [40^\circ, -20^\circ, 0^\circ, 60^\circ, 80^\circ]$; $M = 4$ with $d_t = [-1, -0.75, -0.5, -0.25, 0, 0.25, 0.5, 0.75, 1]\,\lambda$ and $\varepsilon_{m,t} = [10^\circ, 30^\circ, 40^\circ, -20^\circ, 0^\circ, 60^\circ, 80^\circ, 25^\circ, 55^\circ]$.

According to the previous analysis, the maximum number of identifiable targets is the same as the number of transmit array antennas or receive array antennas. Therefore, the number of targets is set to be equal to the number of transmit/ receive array antennas in **Scenario 1**. Then, in order to demonstrate the applicability of the proposed method to non-uniform linear arrays, the transmit/ receive arrays are set to be non-uniform linear arrays in **Scenario 2**. Since Singh's method is only suitable for ULAs with restrictions on inter-element spacing, ULA is considered in **Scenario 3**. Finally, to evaluate the performance of the proposed method under different number of transmit antennas, two numbers of transmit antennas are set in **Scenario 4**.

Simulation 1: In the first simulation, to demonstrate the maximum number of identifiable targets by the proposed method, Fig. 4 provides some estimation results through 50 Monte-Carlo trials, where the signal-to-noise ratio (SNR) is set to 40dB, the number of snapshots is set to 50000, and Scenario 1 is considered. It can be observed that, when both the transmit array and the receive array have 5 antennas, the proposed method can effectively identify 5 targets, which is in accordance with the analysis in part B of Sec. IV, and the eight-dimensional (8-D) parameters can be automatically paired. In addition, Fig. 5 shows the proposed method can accurately estimate the sensors' unknown phase uncertainties.

In the following simulations, the estimation performance is evaluated through the root-mean-square error (RMSE) defined as follows

$$RMSE = \sqrt{\frac{1}{500K}\sum_{k=1}^{K}\sum_{p=1}^{500}\left(\hat{\vartheta}_{p,k} - \vartheta_k\right)^2}, \tag{61}$$

where $\hat{\vartheta}_{p,k}$ represents the estimates of the parameters $\theta_{tk}, \theta_{rk}, r_{tk}, r_{rk}, \gamma_{tk}, \gamma_{rk}, \eta_{tk}$, and η_{rk} at the p-th Monte-Carlo

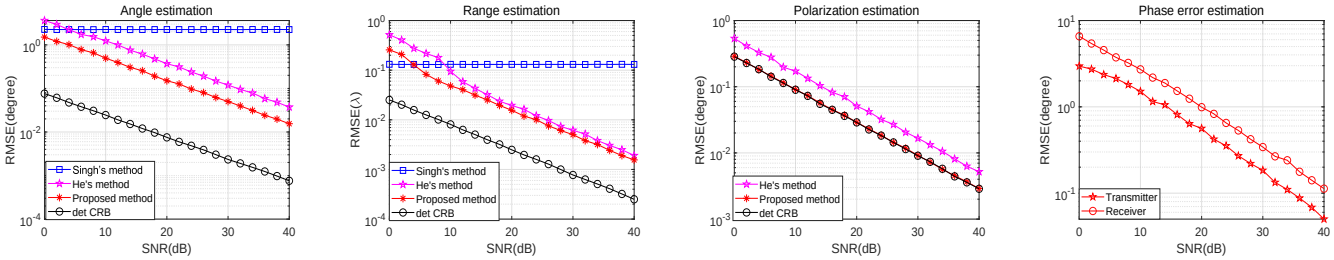

(a) Angle estimation. (b) Range estimation. (c) Polarization estimation. (d) Phase error estimation.

Fig. 6. Estimation performance comparison versus SNR.

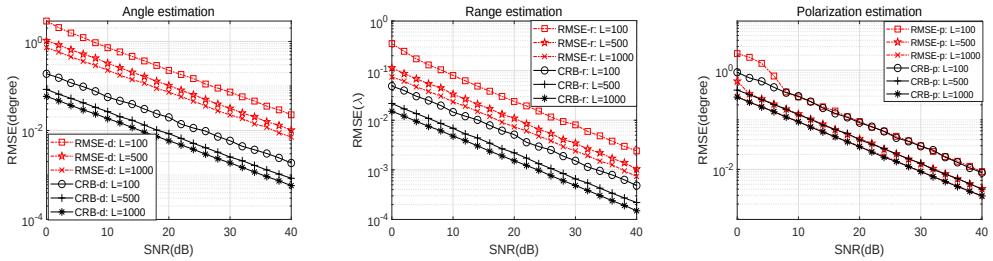

(a) Angle estimation. (b) Range estimation. (c) Polarization estimation.

Fig. 7. RMSE results of the proposed method under different numbers of snapshots.

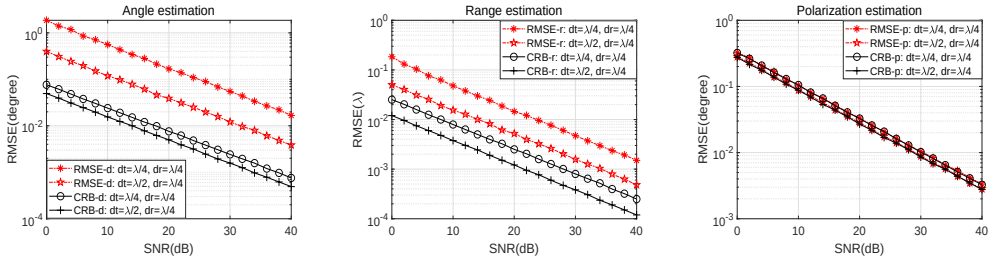

(a) Angle estimation. (b) Range estimation. (c) Polarization estimation.

Fig. 8. RMSE results of the proposed method under different transmit element spacings.

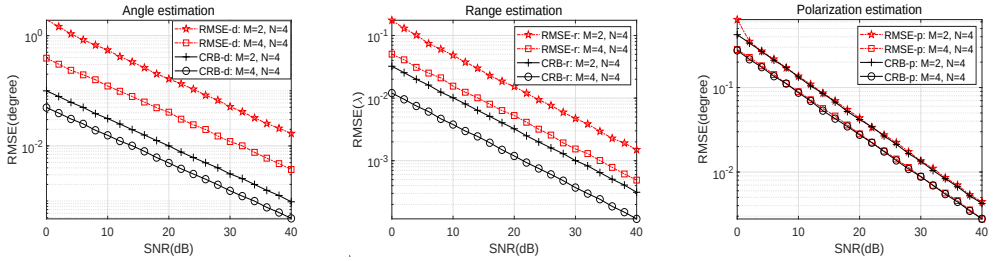

(a) Angle estimation. (b) Range estimation. (c) Polarization estimation.

Fig. 9. RMSE results of the proposed method under different numbers of transmit elements.

trial, while ϑ_k denotes the true value, and the results are obtained based on 500 Monte-Carlo trials.

Simulation 2: In the second simulation, the estimation performance of the proposed method is compared to that of Singh's method [13] and He's method [33], and the CRB is provided as a benchmark. Since Singh's method is only suitable for ULAs with restrictions on inter-element spacing, **Scenario 3** is considered in this simulation. Figs. 6 (a) and (b) illustrate the DOD/DOA and range's estimation result with SNR varying from 0dB to 40dB. As can be seen, the RMSE results of the proposed method decrease significantly with the increase of SNR, while that of the Singh's method stays almost the same with the increase of SNR due to model mismatch errors in the method, i.e., ignoring propagation loss. In addition, it can be seen from Figs. 6 (a), (b) and (c) that the proposed method is more effective than He's method. The reason for a better angle and range estimation performance by the proposed method is that the proposed one utilizes all elements of the transmit/receive arrays, while He's method only utilizes any two elements of the transmit/receive arrays. As for polarization parameter estimation, the estimation performance by employing the PARAFAC method is better than that of the subspace method, which makes fully use of advantages of the PARAFAC model, such as suppressing noise of a strong multi-dimensional nature in array measurements, etc., as indicated in [23]. The estimation performance of phase errors is also examined, and as shown in Fig. 6 (d), the corresponding RMSE decreases as SNR increases.

Simulation 3: In this simulation, performance of the proposed method is examined under different numbers of snapshots (L), where **Scenario 2** is considered. It can be observed from Fig. 7 that the estimation accuracy of angle, range and polarization parameters by the proposed method is the worst for a small number of snapshots L=100. As the number of snapshots increases from L=500 to L=1000, the performance for all parameters improves, as an increasing L provides more time diversity gain.

Simulation 4: In this simulation, the effect of different transmit array element spacings is studied, where **Scenario 3** is considered with additional transmit array element spacing $\lambda/2$ for comparison, that is $d_t = [-2, -1.5, -1, -0.5, 0, 0.5, 1, 1.5, 2]\,\lambda$. Fig. 8 presents the angle, range and polarization estimation results with different transmit array element spacings. It can be clearly seen that the estimation error of angle and range parameters obtained by the proposed method decreases with the increase of the transmit array element spacing, which expands the array aperture. At the same time, it can be observed from Fig. 8 (c) that the performance of polarization estimation remains almost unchanged with increasing transmit array element spacing, which is in consistent with the observation in [33]. In addition, the proposed method has no ambiguity problem with the transmit sensor spacing as large as half wavelength, as only the spatial amplitude ratio is exploited to obtain all the parameters. And the same conclusion can be drawn for different receive array element spacings.

Simulation 5: The performance versus number of transmit antennas is shown in Fig. 9, where **Scenario 4** is considered. It can be seen that when the number of receive array antennas is the same, the estimation error, related to angle, range and polarization parameters, respectively, decreases with the increase of the number of transmit antennas, which improves the space diversity gain for the MIMO system. The same conclusion can be drawn for different numbers of receive antennas, given a fixed number of transmit array antennas.

VI. Conclusion

In this paper, a novel estimation algorithm has been proposed for a bistatic MIMO system considering the exact spatial propagation model, where both the transmitter and the receiver are equipped with COLD arrays to achieve estimation of parameters including DOD, DOA, RFTT, RFTR, TPA, RPA, and phase uncertainties of the transmit and receive arrays. The 8-D parameters are automatically paired and accurately estimated through trilinear decomposition. Besides, the proposed algorithm is suitable for NULAs, and the element spacing does not need to be limited to a quarter or half wavelength as in many cases of traditional methods.

References

[1] Z. Zheng, N. Guo, and W.-Q. Wang, "Angle estimation for bistatic MIMO radar using one-bit sampling via atomic norm minimization," *IEEE Transactions on Aerospace and Electronic Systems*, pp. 1–1, 2022.

[2] F. Xu, M. W. Morency, and S. A. Vorobyov, "DOA estimation for transmit beamspace MIMO radar via tensor decomposition with vandermonde factor matrix," *IEEE Transactions on Signal Processing*, vol. 70, pp. 2901–2917, 2022.

[3] J. Shi, F. Wen, and T. Liu, "Nested MIMO radar: Coarrays, tensor modeling, and angle estimation," *IEEE Transactions on Aerospace and Electronic Systems*, vol. 57, no. 1, pp. 573–585, 2021.

[4] X. Zhang, L. Xu, L. Xu, and D. Xu, "Direction of departure (DOD) and direction of arrival (DOA) estimation in MIMO radar with reduced-dimension MUSIC," *IEEE Communications Letters*, vol. 14, no. 12, pp. 1161–1163, 2010.

[5] D. Chen, B. Chen, and G. Qin, "Angle estimation using ESPRIT in MIMO radar," *Electronics Letters*, vol. 44, pp. 770–771, 2008.

[6] J. Chen, H. Gu, and W. Su, "Angle estimation using ESPRIT without pairing in MIMO radar," *Electronics Letters*, vol. 44, pp. 1422–1423, 2008.

[7] D. Nion and N. D. Sidiropoulos, "Tensor algebra and multidimensional harmonic retrieval in signal processing for MIMO radar," *IEEE Transactions on Signal Processing*, vol. 58, no. 11, pp. 5693–5705, 2010.

[8] E. Zhou, H. Jiang, and H. Qi, "4-D parameter estimation in bistatic MIMO radar for near-field target localization," in *2015 IEEE International Wireless Symposium (IWS 2015)*, 2015, pp. 1–4.

[9] A. M. Molaei, P. del Hougne, V. Fusco, and O. Yurduseven, "Efficient joint estimation of DOA, range and reflectivity in near-field by using mixed-order statistics and a symmetric MIMO array," *IEEE Transactions on Vehicular Technology*, vol. 71, no. 3, pp. 2824–2842, 2022.

[10] Z. Zheng, M. Fu, W.-Q. Wang, and H. C. So, "Symmetric displaced coprime array configurations for mixed near- and far-field source localization," *IEEE Transactions on Antennas and Propagation*, vol. 69, no. 1, pp. 465–477, 2021.

[11] H. Chen, Z. Jiang, W. Liu, Y. Tian, and G. Wang, "Conjugate augmented decoupled 3-D parameters estimation method for near-field sources," *IEEE Transactions on Aerospace and Electronic Systems*, vol. 58, no. 5, pp. 4681–4689, 2022.

[12] C. Cheng, S. Liu, H. Wu, and Y. Zhang, "An efficient maximum-likelihood-like algorithm for near-field coherent source localization," *IEEE Transactions on Antennas and Propagation*, vol. 70, no. 7, pp. 6111–6116, 2022.

[13] P. Singh, Y. Wang, and P. Charg, "Bistatic MIMO radar for near field source localisation using PARAFAC," *Electronics Letters*, vol. 52, no. 12, pp. 1060–1061, 2016.

[14] I. Podkurkov, L. Hamidullina, E. Traikov, M. Haardt, and A. Nadeev, "Tensor-based near-field localization in bistatic MIMO radar systems," in *WSA 2018; 22nd International ITG Workshop on Smart Antennas*, 2018, pp. 1–8.

[15] L. Khamidullina, I. Podkurkov, and M. Haardt, "Conditional and unconditional cramer-rao bounds for near-field localization in bistatic MIMO radar systems," *IEEE Transactions on Signal Processing*, vol. 69, pp. 3220–3234, 2021.

[16] A. Nehorai and E. Paldi, "Vector-sensor array processing for electromagnetic source localization," *IEEE Transactions on Signal Processing*, vol. 42, no. 2, pp. 376–398, 1994.

[17] A. Tanveer, X. Zhang, and W. Zheng, "Direction of arrival estimation for coprime electromagnetic vector sensor arrays via minimum distance criterion based on PARAFAC analysis," *IET Radar, Sonar Navigation*, vol. 10, pp. 65–73, 2018.

[18] H. Chen, W. Wang, and W. Liu, "Augmented quaternion ESPRIT-pype DOA estimation with a crossed-dipole array," *IEEE Communications Letters*, vol. 24, no. 3, pp. 548–552, 2020.

[19] K. Wong and M. Zoltowski, "Uni-vector-sensor ESPRIT for multisource azimuth, elevation, and polarization estimation," *IEEE Transactions on Antennas and Propagation*, vol. 45, no. 10, pp. 1467–1474, 1997.

[20] X. Guo, S. Miron, D. Brie, S. Zhu, and X. Liao, "A CANDECOMP/PARAFAC perspective on uniqueness of DOA estimation using a vector sensor array," *IEEE Transactions on Signal Processing*, vol. 59, no. 7, pp. 3475–3481, 2011.

[21] C. Gu, J. He, H. Li, and X. Zhu, "Target localization using MIMO electromagnetic vector array systems," *Signal Processing*, vol. 93, pp. 2103–2107, 2013.

[22] S. Chintagunta and P. Ponnusamy, "2D-DOD and 2D-DOA estimation using the electromagnetic vector sensors," *Signal Processing*, vol. 147, 2018.

[23] F. Wen, J. Shi, and Z. Zhang, "Joint 2D-DOD, 2D-DOA, and polarization angles estimation for bistatic EMVS-MIMO radar via PARAFAC analysis," *IEEE Transactions on Vehicular Technology*, vol. 69, no. 2, pp. 1626–1638, 2020.

[24] H. Ma, H. Tao, J. Su, and B. Liao, "DOD/DOA and polarization estimation in MIMO systems with spatially spread dipole quints," *IEEE Communications Letters*, vol. 24, no. 1, pp. 99–102, 2020.

[25] B. Friedlander, "Localization of signals in the near-field of an antenna array," *IEEE Transactions on Signal Processing*, vol. 67, no. 15, pp. 3885–3893, 2019.

[26] J. He, L. Li, T. Shu, and T.-K. Truong, "Mixed near-field and far-field source localization based on exact spatial propagation geometry," *IEEE Transactions on Vehicular Technology*, vol. 70, no. 4, pp. 3540–3551, 2021.

[27] T. Shu, J. He, and L. Li, "Near-field passive localization and gain-phase compensation with partly calibrated arrays," *IEEE Transactions on Aerospace and Electronic Systems*, vol. 58, no. 1, pp. 712–719, 2022.

[28] J. He, T. Shu, L. Li, and T.-K. Truong, "Mixed near-field and far-field localization and array calibration with partly calibrated arrays," *IEEE Transactions on Signal Processing*, vol. 70, pp. 2105–2118, 2022.

[29] K. Yin, C. Gao, and Y. Dai, "Near-field localization based on exact model with a linear COLD array," in *2022 IEEE Radar Conference (RadarConf22)*, 2022, pp. 1–6.

[30] J. He, L. Li, and T. Shu, "Localization of near-field sources for exact source-sensor spatial geometry," *IEEE Signal Processing Letters*, vol. 27, pp. 1040–1044, 2020.

[31] J. Li, P. Stoica, and D. Zheng, "Efficient direction and polarization estimation with a cold array," *IEEE Transactions on Antennas and Propagation*, vol. 44, no. 4, pp. 539–547, 1996.

[32] J. He, M. O. Ahmad, and M. N. S. Swamy, "Near-field localization of partially polarized sources with a cross-dipole array," *IEEE Transactions on Aerospace and Electronic Systems*, vol. 49, no. 2, pp. 857–870, 2013.

[33] J. He, L. Li, and T. Shu, "Near-field parameter estimation for polarized source using spatial amplitude ratio," *IEEE Communications Letters*, vol. 24, no. 9, pp. 1961–1965, 2020.

[34] J. Du, J. Dong, L. Jin, and F. Gao, "Bayesian robust tensor factorization for angle estimation in bistatic MIMO radar with unknown spatially colored noise," *IEEE Transactions on Signal Processing*, vol. 70, pp. 6051–6064, 2022.

[35] R. Bro, "Parafac. tutorial and applications," *Chemometrics and Intelligent Laboratory Systems*, vol. 38, no. 2, pp. 149–171, 1997.

[36] R. Bro, N. D. Sidiropoulos, and G. B. Giannakis, "A fast least squares algorithm for separating trilinear mixtures," *Proc Ica'99 Aussois*, pp. 289–294, 1999.

[37] J. B. Kruskal, "Three-way arrays: rank and uniqueness of trilinear decompositions, with application to arithmetic complexity and statistics," *Linear Algebra and its Applications*, vol. 18, no. 2, pp. 95–138, 1977.

Hua Chen (Member, IEEE) received the M.Eng. degree and Ph.D. degree in Information and Communication Engineering from Tianjin University, Tianjin, China, in 2013 and 2017, respectively. He is now as an Associate Professor in Faculty of Information Science and Engineering, Ningbo University, China. His research interests include array signal processing, MIMO radar. He is currently an Associate Editor for Circuits, Systems, and Signal Processing.

Weilong Wang received the B.S. degree in electronic information science and technology in 2020 from Henan Agricultural University, Zhengzhou, China. He is currently working toward the M.S. degree in information and communication engineering at the School of Faculty of Information Science and Engineering, Ningbo University. His research focuses on MIMO radar.

Wei Liu (S'01-M'04-SM'10) received his BSc and LLB. degrees from Peking University, China, in 1996 and 1997, respectively, MPhil from the University of Hong Kong in 2001, and PhD from University of Southampton, UK, in 2003. He then worked as a postdoc first at Southampton and later at Imperial College London. In September 2005, he joined the Department of Electronic and Electrical Engineering, University of Sheffield, UK, first as a Lecturer and then a Senior Lecturer. Since September 2023, he has been a Reader at the School of Electronic Engineering and Computer Science, Queen Mary University of London, UK. He has published 390+ journal and conference papers, five book chapters, and two research monographs titled "Wideband Beamforming: Concepts and Techniques" (Wiley, March 2010) and "Low-Cost Smart Antennas" (Wiley, March 2019), respectively. His research interests cover a wide range of topics in signal processing, with a focus on sensor array signal processing and its various applications, such as robotics and autonomous systems, human computer interface, radar, sonar, and wireless communications.

He is a member of the Digital Signal Processing Technical Committee of the IEEE Circuits and Systems Society (Chair from May 2022) and the Sensor Array and Multichannel Signal Processing Technical Committee of the IEEE Signal Processing Society (Chair for 2021-2022), and an IEEE Distinguished Lecturer for the Aerospace and Electronic Systems Society (2023-2024). He also acted as an associate editor for IEEE Trans. on Signal Processing, IEEE Access, and Journal of the Franklin Institute (2021-2023), and currently he is an Executive Associate Editor-in-Chief of the Frontiers of Information Technology and Electronic Engineering.

Ye Tian (S'13-M'19) received the B.S. and Ph.D. degrees from the College of Communication Engineering, Jilin University, Changchun, China, in 2009 and 2014, respectively. He won a Huawei scholarship in 2013 and was selected as a young top talent by the Hebei Provincial Department of Education in 2016. He is currently an Associate Professor in Faculty of Information Science and Engineering, Ningbo University. He has published more than 30 international peer-reviewed journal/conference papers and more than 10 patents. His research interests include array signal processing, autonomous vehicle positioning, massive MIMO as well as large-dimensional random matrix theory.

Gang Wang (Senior Member, IEEE) received the B.Eng. degree from Shandong University, Jinan, China, and the Ph.D. degree from Xidian University, Xian, China, both in electrical engineering, in 2006 and 2011, respectively. He joined Ningbo University, Ningbo, China, in January 2012, where he is currently a full Professor. Form January 2014 to April 2014, he was a Research Associate at the Chinese University of Hong Kong. From June 2018 to June 2019, he was a Visiting Scholar at the University of Missouri, Columbia, USA. His research interests are in the areas of target localization and tracking in wireless networks, array singal processing, and robust ellipse fitting in image processing.

Dr. Wang is the winner of the Distinguished Young Scholars of Zhejiang Provincial Natural Science Foundation. He serves as Handling Editor for Digital Signal Processing (Elsevier) and Signal Processing (Elsevier), and Associate Editor for IEEE Transactions on Aerospace and Electronic Systems. He is a member of the IEEE Signal Processing Society Sensor Array and Multichannel (SAM) Technical Committee.